ACS APPLIED MATERIALS & INTERFACES

Research Article

www.acsami.org

Porous Carbon Nanosheets Codoped with Nitrogen and Sulfur for Oxygen Reduction Reaction in Microbial Fuel Cells

Heyang Yuan,[†,§] Yang Hou,[‡,§] Zhenhai Wen,[‡] Xiaoru Guo,[‡] Junhong Chen,[*,‡] and Zhen He[*,†]

[†]Department of Civil and Environmental Engineering, Virginia Polytechnic Institute and State University, Blacksburg, Virginia 24061, United States

[‡]Department of Mechanical Engineering, University of Wisconsin—Milwaukee, 3200 North Cramer Street, Milwaukee, Wisconsin 53211, United States

ABSTRACT: In this work, a simple synthesis strategy has been developed for the preparation of nitrogen- and sulfur-codoped porous carbon nanosheets (N/S-CNS) as a cathode catalyst for microbial fuel cells (MFCs). The as-prepared N/S-CNS showed favorable features for electrochemical energy conversion such as high surface area (1004 m^2 g^{-1}), defect structure, and abundant exposure of active sites that arose primarily from porous nanosheet morphology. Benefiting from the unique nanostructure, the resulting nanosheets exhibited effective electrocatalytic activity toward oxygen reduction reaction (ORR). The onset potential of the N/S-CNS in linear-sweep voltammetry was approximately −0.05 V vs Ag/AgCl in neutral phosphate buffer saline. Electrochemical impedance spectroscopy showed that the ohmic and charge-transfer resistance of the codoped catalyst were 1.5 and 14.8 Ω, respectively, both of which were lower than that of platinum/carbon (Pt/C). Furthermore, the electron-transfer number of the N/S-CNS was calculated to be ∼3.5, suggesting that ORR on the catalyst proceeds predominantly through the favorable four-electron pathway. The MFC with N/S-CNS as a cathode catalyst generated current density (6.6 A m^{-2}) comparable to that with Pt/C (7.3 A m^{-2}). The high durability and low price indicate that N/S-CNS can be a competitive catalyst for applications of MFCs.

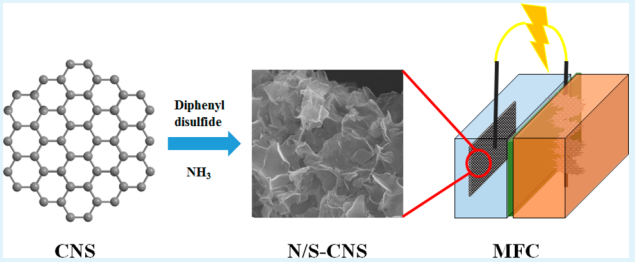

KEYWORDS: *carbon nanosheets, nitrogen doping, sulfur doping, oxygen reduction reaction, microbial fuel cells*

INTRODUCTION

The oxygen reduction reaction (ORR) is one of the most critical reactions for electrochemical systems. Because ORR is sluggish, platinum is widely used as a catalyst in laboratory experiments but is economically not feasible for large-scale applications, which poses a major challenge for fuel-cell applications.[1] Nonprecious metals such as manganese, iron, and cobalt have also been modified, and efficient catalysis has been obtained.[2,3] However, the long-term stability of these metal catalysts remains to be examined.

Carbon materials are of great interest for fuel cells because of their low cost and high stability.[4,5] Nitrogen-doped carbon catalysts (e.g., carbon nanotubes, nanosheets, graphene, etc.) exhibit abundant defect sites, high specific surface area, and high conductivity and thus have drawn great attention in recent years.[6−8] Enhanced ORR catalysis using nitrogen-doped carbon materials has therefore been extensively reported in previous studies.[9,10] In addition to nitrogen, heteroatoms such as boron, sulfur, and phosphorus have also been doped in carbon-based materials and noticeably enhanced ORR catalysis.[11,12] The catalytic activity was reported to be further improved by dual doping of nitrogen and sulfur,[13,14] and the specific surface area of a nitrogen−sulfur (N/S)-codoped three-dimensional (3D) carbon foam reached 850 m^2 g^{-1}.[15] While the synergetic effects of the dopants and the ORR mechanism remained to be explored, dual-doped N/S carbon materials with outstanding ORR catalytic activity may hold great promise for the development of fuel cells.

Another perspective of fuel cells is to generate energy from renewable resources such as wastewater. Wastewater is increasingly recognized as a green resource because of the potential energy and nutrient that it contains.[16] The chemical energy stored in organic matters in wastewater can be directly converted into electricity by microbial fuel cells (MFCs).[17] In the anode of an MFC, exoelectrogens degrade organics and respire by releasing electrons extracellularly to the anode electrode.[18] When proper electron acceptors (e.g., oxygen) are used in the cathode and the overall reaction of the cell is thermodynamically favorable, the electrons will flow spontaneously through an external circuit to the cathode.[19] As such, wastewater treatment and electricity generation are achieved simultaneously. Similar to chemical fuel cells, oxygen is a common electron acceptor because of its availability and high reduction potential. Therefore, advances in carbon-based materials for ORR catalysis may play an important role in sustainable water and wastewater treatment in the future. A

Received: June 10, 2015
Accepted: August 3, 2015
Published: August 3, 2015

DOI: 10.1021/acsami.5b05144
ACS Appl. Mater. Interfaces 2015, 7, 18672−18678

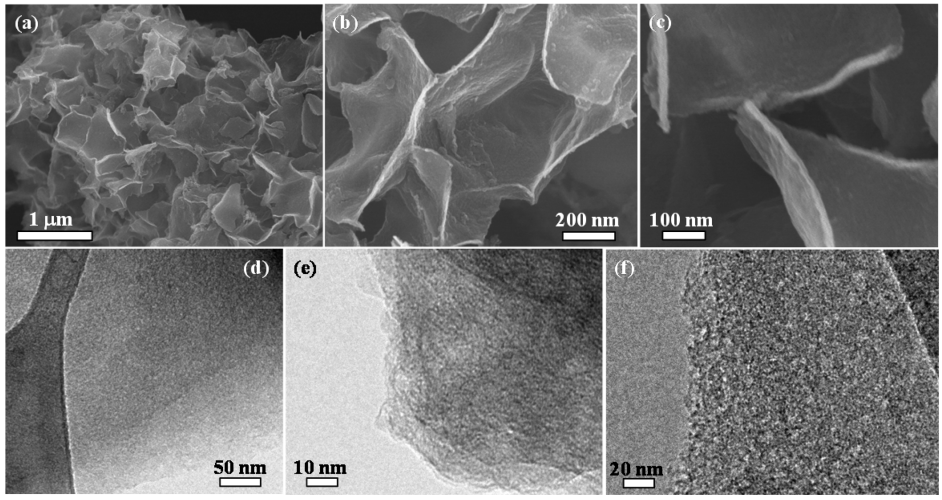

Figure 1. FESEM (a–c) and TEM (d–f) images of the N/S-CNS.

variety of carbon-based materials, including activated carbon[20–22] and grapheme,[23] have been studied as cathode catalysts for MFCs and show great promise in terms of performance and stability.

In this work, we have demonstrated the simple synthesis of N/S-codoped porous carbon nanosheets (N/S-CNS) with abundant active sites and high surface area. The ORR catalysis of the as-prepared catalysts was studied by linear-sweep voltammetry (LSV), electrochemical impedance spectroscopy (EIS), and rotating-disk electrode (RDE) measurement. To better understand the catalysis performance, the catalysts were further examined in an MFC. The present work is expected to provide insight into the dual doping of nitrogen and sulfur in carbon materials and the application of such catalysts in MFCs for energy-efficient wastewater and/or water treatment.

METHODS AND MATERIALS

Synthesis of N/S-CNS. To synthesize the catalysts, 1 g of potassium citrate was annealed in an argon atmosphere at 850 °C for 2 h at a heating rate of 2 °C min^{-1}.[24] The porous CNSs were generated by further treatment of the products as-obtained above with a 0.5 M H_2SO_4 solution overnight, followed by washing with deionized water and vacuum drying, with a yield of about 41%. Next, the obtained porous CNSs were dissolved into 10 mL of ethanol, followed by the addition of 0.5 g of diphenyl disulfide under stirring. Then, the solvent was slowly evaporated at 50 °C. The remaining powder was further heated at 750 °C at a rate of 2 °C min^{-1} and held at that temperature for 2 h under an ammonia atmosphere, resulting in the formation of porous N/S-CNS. For comparison, CNSs were also doped solely with nitrogen or sulfur.

Characterization. Microstructures of the samples were examined using transmission electron microscopy (TEM; Hitachi H 9000 NAR) and field-emission scanning electron microscopy (FESEM; Hitachi S-4800). X-ray diffraction (XRD) data were obtained with a Scintag XDS 2000 powder X-ray diffractometer (Cu Kα radiation source, λ = 1.5418 Å). Raman spectroscopy was recorded on a Renishaw 1000B spectrometer with laser excitation (wavelength = 633 nm). X-ray photoelectron spectroscopy (XPS) analysis was performed on an HP 5950A spectrometer equipped with Mg Kα as the source. The Brunauer–Emmett–Teller (BET) surface area was determined by using a Micromeritics ASAP 2010 instrument with N_2 adsorption.

Electrochemical Analysis. A total of 5 mg of the synthesized catalysts was mixed with 40 μL of a Nafion perfluorinated ion-exchange resin (Sigma-Aldrich, St. Louis, MO) and 60 μL of deionized water and applied to a carbon cloth (PANEX30PW03; Zoltek Corp., St. Louis, MO) with an area of 1 cm^2 to obtain a loading rate of 5 mg cm^{-2}. After coating, the carbon cloth was dried in a fume hood for 24 h and was ready for use.[25] An 1 cm^2 carbon cloth coated with 5 mg cm^{-2} of Pt/C (10 wt % Platinum on Carbon Vulcan; Fuel Cell Earth LLC, Woburn, MA) was prepared by the same method and served as the control. These electrodes were examined as the working electrode in a three-electrode cell containing 120 mL of 0.1 M phosphate buffer saline (PBS; 5.3 g L^{-1} KH_2PO_4 and 10.7 g L^{-1} K_2HPO_4), with a platinum wire (CH Instruments, Inc., Bee Cave, TX) as the counter electrode and Ag/AgCl (CH Instruments, Inc., Bee Cave, TX) as the reference electrode. LSV was measured with a potentiostat (Reference600; Gamry Instruments, Warminster, PA) at a scan rate of 10 mV s^{-1}. EIS was conducted at the open-circuit voltage with a sinusoidal perturbation of 10 mV and the frequency ranging from 10^{-3} to 10^5 Hz. The data were fitted with Gamry *Echem Analyst* software. The electrodes were rinsed with deionized water and air-dried before each test. The electrolyte was aerated for 15 min prior to each experiment and kept aerating in the headspace during the course of the experiments.

RDE measurements were conducted in the same three-electrode cell to study the ORR mechanism. A glass carbon tip (diameter 3 mm; BASI, West Lafayette, IN) was polished with alumina slurry (PK-4 Polishing kit; BASI, West Lafayette, IN) to obtain a mirrorlike surface and then washed with deionized water and ethanol. An ink solution with a concentration of 100 mg mL^{-1} was prepared by mixing 10 mg of the catalyst powder with 40 μL of Nafion and 60 μL of deionized water. After 10 min of ultrasonication, 3.6 μL of the ink solution was pipetted on the glassy-carbon RDE tip at a loading rate of ~5 mg cm^{-2}. The current density was recorded at a scan rate of 10 mV s^{-1}, and the rotation rate was varied from 100 to 1600 rpm (RDE-2; BASI, West Lafayette, IN). To maintain a constant O_2 level, the electrolyte was aerated using an air pump (Aqua Supreme Air Pump 2 W; Danner Manufacturing, Islandia, NY) during the measurement. The electrolyte was then purged with N_2 for 15 min, and LSV was conducted to obtain the baseline for each catalyst. The baseline was subtracted, and the electron-transfer number (n) was calculated from the slope of the Koutecký–Levich (K–L) plot:[26]

$$\frac{1}{i} = \frac{1}{i_K} + \frac{1}{0.62nFAD_{O_2}^{2/3}\nu^{-1/6}C}\frac{1}{\omega^{1/2}} \quad (1)$$

where i_K is the kinetic current (A), F is the Faradaic constant (96485 C mol^{-1}), A is the electrode area (0.071 cm^2), D_{O_2} is the diffusion coefficient of O_2 in 0.1 M PBS (2.15 cm^2 s^{-1}),[27] ν is the kinematic viscosity of the electrolyte (0.01 cm^2 s^{-1}), C is the O_2 centration in the electrolyte (2.6×10^{-7} mol cm^{-3}) measured using a DO meter (Orion Star A213; Thermo Fisher Scientific Inc., Waltham, MA), and ω is the angular rotation velocity (rad s^{-1}). The durability of the catalysts was investigated by performing RDE at 1600 rpm after 3000 and 6000

DOI: 10.1021/acsami.5b05144
ACS Appl. Mater. Interfaces 2015, 7, 18672–18678

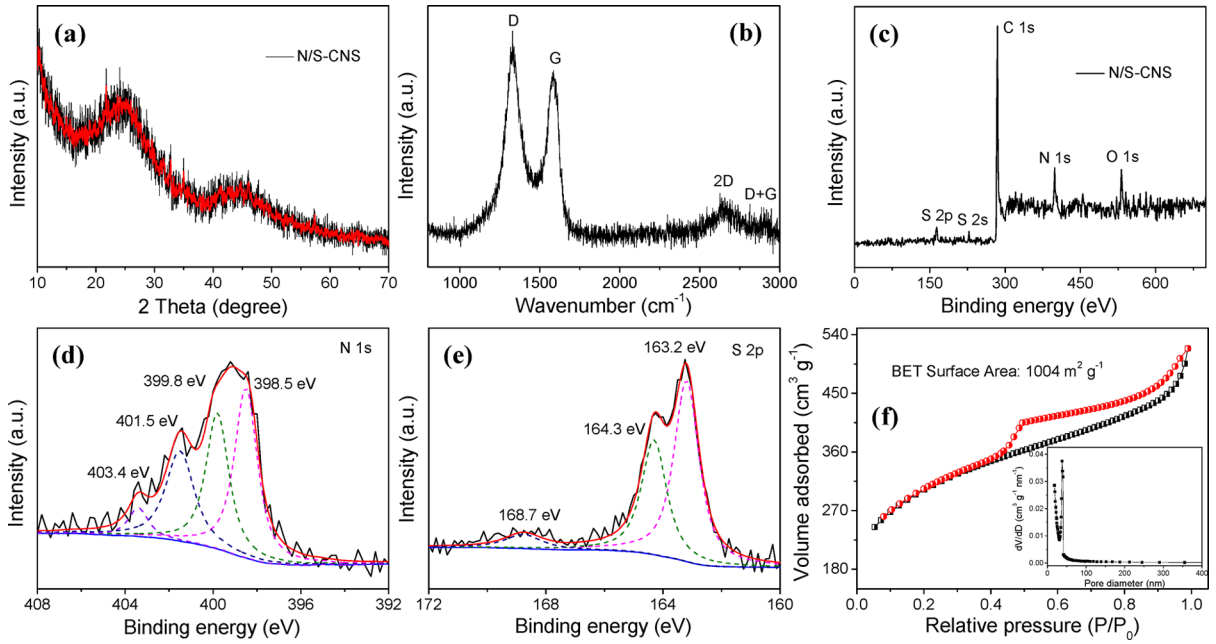

Figure 2. XRD pattern (a), Raman spectrum (b), XPS sweep scan (c), high-resolution N 1s XPS spectrum (d), high-resolution S 2p XPS spectrum (e), N_2 adsorption/desorption isotherm (f) for the N/S-CNS. Inset to panel f: corresponding pore-size distribution.

cycles of cyclic voltammetry (scan rate 100 mV s^{-1}). All electrochemical experiments were conducted three times at room temperature.

MFC Construction and Operation. A two-chamber MFC was constructed by connecting two glass bottles with a cation-exchange membrane as the separator (CMI-7000S; Membranes International, Inc., Ringwood, NJ). The liquid volumes of the anodic and cathodic chambers were 130 and 140 mL, respectively. The anode electrode was a carbon brush (Gordon Brush Mfg. Co., Inc., Commerce, CA) that had been cultivated in the MFC for over 1 month. The anolyte contained the following (per liter of deionized water): sodium acetate, 1.0 g; NaCl, 0.5 g; $MgSO_4$, 0.015 g; $CaCl_2$, 0.02 g; KH_2PO_4, 2.65 g; K_2HPO_4, 5.35 g; $NaHCO_3$, 1.0 g; trace element, 1.0 mL.[28] The carbon cloth coated with the catalysts was examined as a cathode electrode. The catholyte was a 0.1 M PBS solution. The anode and cathode electrodes were connected through a 1-Ω resistor (HARS-X-3-0.001; IET Laboratories, Inc., Roslyn Heights, NY). The voltage on the resistor was recorded by a digital multimeter (2700; Keithley Instruments, Inc., Cleveland, OH) at a time interval of 5 min. The current of the MFC was calculated according to Ohm's law. Duplicate polarization curves were measured using the potentiostat at a scan rate of 0.2 mV s^{-1}. The MFC was operated under batch mode at room temperature. The anolyte and catholyte were changed every 24 h. Both the anode and cathode were stirred, and the cathode chamber was aerated.

RESULTS AND DISCUSSION

Characterization of the Catalysts. The morphology and microstructure of an as-prepared N/S-CNS was examined by FESEM and TEM. The product is of two-dimensional (2D) nanosheet morphology with lateral width ranging from hundreds of nanometers to several micrometers (Figure 1a), and the thickness is approximately 23 nm (Figure 1b,c). The N/S-CNS exhibited a highly interconnected 3D framework of randomly stacked nanosheets with porous architecture, similar to the previously reported crumpled graphene particle,[10] which may be favorable for access of the electrolyte and shortens the transport distance between the electrode and electrolyte.[29] TEM analyses further confirmed the layered morphology of the as-synthesized N/S-CNS (Figure 1d), which agrees well with the FESEM observation. The partially crinkled nature may have originated from the defective structures formed by nitrogen and sulfur doping (Figure 1e).[30] Many alternative dark and light areas from the high-resolution TEM image in Figure 1f clearly reveal the presence of numerous pores on the surface of the N/S-CNS.

The crystal structure of the N/S-CNS was studied by XRD measurements. Two broad diffraction peaks centered at around 24.6° and 44.7° can be well assigned to diffraction from the (002) and (101) planes of graphite carbon, respectively,[31] indicating a partial graphitization structure (Figure 2a). The Raman spectrum of the N/S-CNS shows two main peaks centered at 1331 and 1584 cm^{-1}, corresponding to the D and G bands, respectively (Figure 2b). The D band results from the structurally disordered carbon atoms, whereas the G band corresponds to the vibration mode (E_{2g}) for sp^2-hybridized graphitic carbon.[32] The intensity ratio of the D band to the G band (I_D/I_G) is about 1.17, indicating a high degree of disorder,[33] owing to the incorporation of defects by nitrogen and sulfur doping. The smaller peaks at 2660 and 2909 cm^{-1} can be assigned to a combination of 2D and D + G bands.[34,35]

The chemical composition of N/S-CNS was characterized by XPS. Figure 2c presents the survey scan spectrum of the nanosheets with characteristic spectra of C 1s, N 1s, S 2p, S 2s, and O 1s, confirming that nitrogen and sulfur have been successfully codoped into the CNS. The contents of the nitrogen and sulfur elements in the sample are calculated to be 4.6 and 2.4 atom %, respectively. The complex N 1s spectrum could be further deconvoluted into four peaks at 398.5, 399.8, 401.5, and 403.4 eV, corresponding to pyridinic, pyrrolic, graphitic, and oxidized nitrogen, respectively (Figure 2d).[36,37] The high-resolution S 2p peak of the N/S-CNS can be resolved into three different peaks. The former two peaks at 163.2 and 164.3 eV are in agreement with the reported S $2p_{3/2}$ and S $2p_{1/2}$ (Figure 2e),[38] which are attributed to sulfur binding in −C−S− and conjugated −C═S− bonds, respectively.[39] The third peak at 168.7 eV results from oxidized sulfur.[40] The typical N_2

DOI: 10.1021/acsami.5b05144
ACS Appl. Mater. Interfaces 2015, 7, 18672−18678

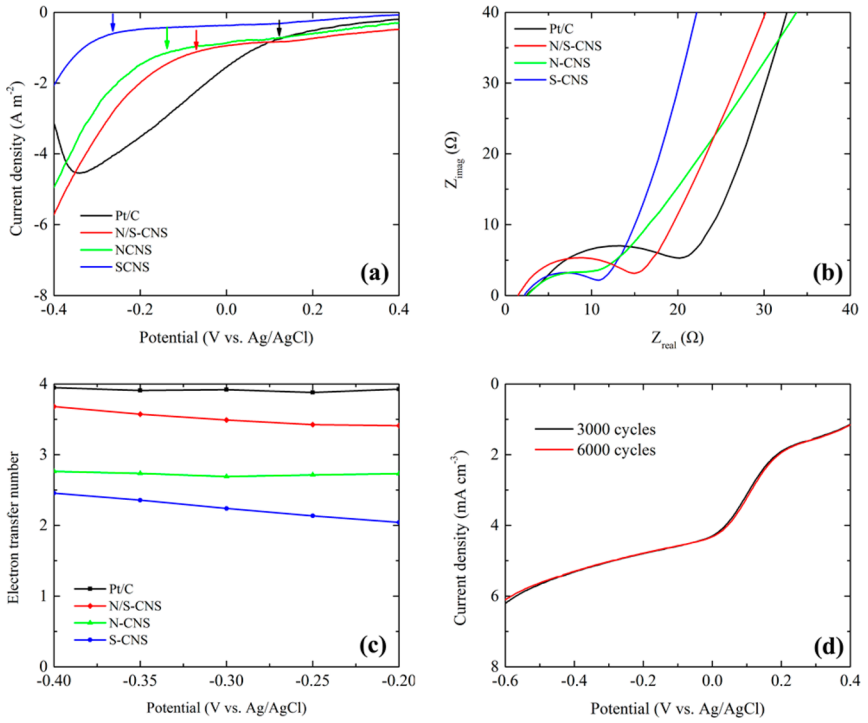

Figure 3. (a) LSV (scan rate of 10 mV s^{-1}) in 0.1 M PBS (arrows indicating the onset potential), (b) EIS in 0.1 M PBS, (c) electron-transfer number calculated from the RDE measurement, and (d) LSV of the N/S-CNS at 1600 rpm after 3000 and 6000 cycles.

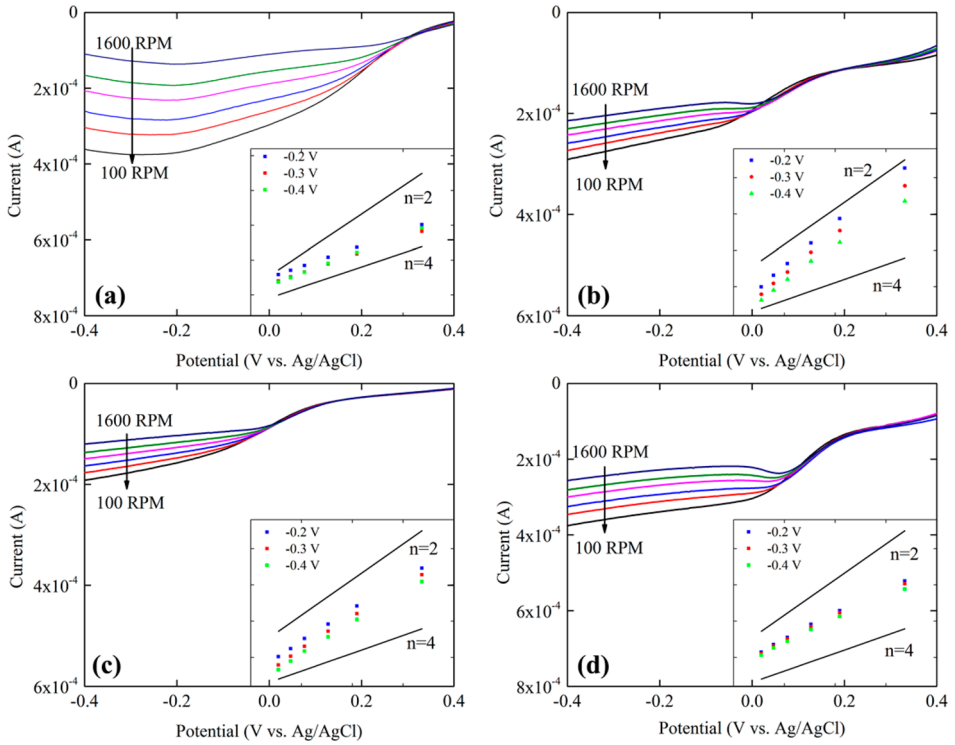

Figure 4. RDE results of (a) Pt/C, (b) S-CNS, (c) N-CNS, and (d) N/S-CNS. Insets: K–L plots at −0.2, −0.3, and −0.4 V vs Ag/AgCl derived from the RDE results. The *y* axis of the insets indicates i^{-1}, and the *x* axis indicates $\omega^{-1/2}$.

adsorption/desorption curve of the resulting N/S-CNS exhibits a type IV adsorption isotherm, indicating that the nanosheets possess porous structures. The BET surface area of the N/S-CNS is estimated to be about 1004 m^2 g^{-1} with a pore volume of 0.8 cm^3 g^{-1} (Figure 2f), which is much higher than those reported for nitrogen- and sulfur-doped graphene materials (typically in the range of 220−820 m^2 g^{-1}).[30,41−44] It is believed that the porous materials with a high BET surface area would provide more active sites and thus improve the ORR activity.[45,46]

Electrochemical Performance. It can be seen in Figure 3a that the onset potential (i.e., the potential at which the onset of

DOI: 10.1021/acsami.5b05144
ACS Appl. Mater. Interfaces 2015, 7, 18672−18678

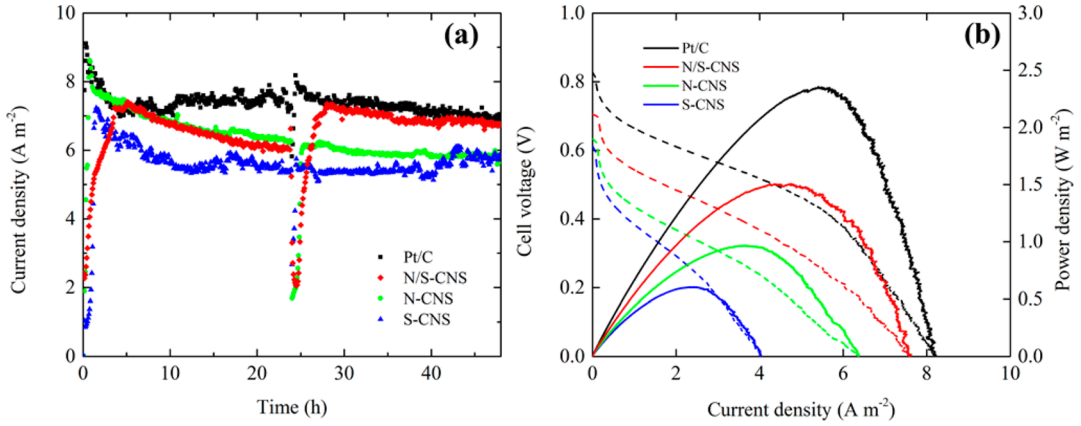

Figure 5. (a) Current density and (b) polarization curves of the MFC with different catalysts.

the electrochemical current occurs[26]) of the N/S-CNS for ORR occurs at −0.05 V vs Ag/AgCl, which is approximately 0.15 V later than that of Pt/C but distinctly earlier than that of CNS solely doped with nitrogen or sulfur, indicating that dual doping of the heteroatoms successfully enhanced the ORR catalysis. These results are consistent with the RDE measurement, in which the onset potential of N/S-CNS occurs at 0.2 V vs Ag/AgCl (Figure 4d), whereas Pt/C shows catalysis at ∼0.3 V vs Ag/AgCl (Figure 4a). The EIS results suggest that CNS is slightly more conductive than Pt/C (Figure 3b). Moreover, the charge-transfer resistance of N/S-CNS (14.8 Ω) is also lower than that of Pt/C (22.3 Ω). The reason that N/S-CNS shows lower resistance than Pt/C but exhibits less catalytic activity (i.e., more negative onset potential) is probably because Pt and CNS catalyze ORR through different pathways. Previous studies proposed that ORR could proceed through a one-step four-electron pathway or the less efficient two-electron pathway.[1]

To gain insight into the ORR mechanisms of N/S-CNS, RDE was carried out in the same electrolyte (Figure 4). The electron-transfer number of N/C-CNS calculated from the RDE results ranged from 3.41 to 3.68 depending on the potential applied (Figure 3c), meaning that ORR on N/S-CNS predominantly followed a four-electron route, but a two-electron pathway is also involved. In contrast, two-electron transfer is likely to be the major mechanism of ORR on N-CNS and S-CNS (Figure 3c). These results are in agreement with the previous findings in which the electron-transfer number of codoped carbon foam or graphene is close to that of Pt/C.[44,47,48]

It has been previously discussed that nitrogen doping may lead to a relatively high positive charge density of the carbon atoms, thereby enhancing the ORR activity.[49] The three nitrogen species also contribute differently to ORR catalysis: pyridinic and pyrrolic nitrogen favors a four-electron pathway, whereas graphitic nitrogen adsorbs OOH and reduces O_2 to H_2O_2 via a two-electron pathway.[21,23] For sulfur doping, because carbon and sulfur atoms have similar electronegativity, spin density may play a more important role and thus sulfur atoms are believed to be the active center.[12] An increased activity of carbon atoms was observed by the simultaneous incorporation of nitrogen and sulfur and attributed to the induced asymmetrical spin and charge density.[14] However, the structures and the consequent synergetic effects of N/S-codoped carbon catalysts may differ because of the different synthesis procedures. Moreover, the specific surface area and defect sites of the carbon materials may also contribute to the overall catalytic behavior. Therefore, the detailed mechanisms of the N/S-doped porous CNSs prepared in the present study warrant further studies. In addition to the remarkable ORR catalysis, the N/S-CNS showed excellent durability because negligible change could be observed after 3000 and 6000 cycles of scan (Figure 3d). These results collectively demonstrate that the N/S-CNS may be a promising ORR catalyst for fuel-cell applications.

MFC Performance. It is worth noting that the catalytic performance in a defined three-electrode system may be different from that in an aerated MFC cathode, where factors such as proton transfer and oxygen diffusion may exert effects on the catalysis. Thus, the catalysts were examined in an MFC with 0.1 M PBS as the catholyte to mimic real situations. The current density of the MFC for all catalysts decreased steadily over time because of the consumption of substrates, dropped drastically at 24 h because of the renewal of electrolyte, and rapidly recovered to the previous level (Figure 5a). This typical current profile implies that the MFC anode has been well cultivated and had little effect on the investigation of the cathode electrode.[25] Similar to the LSV results, the current density followed this order: Pt/C > N/S-CNS > N-CNS > S-CNS. The MFC with Pt/C generated the highest average current density of 7.3 A m^{-2}, followed by 6.6 A m^{-2} of N/S-CNS. The N/S-CNS performed slightly better in the second cycle than it did in the first one and yielded a current density comparable to that of Pt/C possibly because of some activation processes of the catalyst.

The open-circuit voltage and short-circuit current density of N/S-CNS were measured as 0.70 V and 7.6 A m^{-2} (Figure 5b), respectively, both of which were slightly lower than those of Pt/C. As a consequence, the maximum power density calculated from the polarization curve was 1.5 W m^{-2} for N/S-CNS and 2.3 W m^{-2} for Pt/C. Interestingly, it can be seen from Figure 5b that, at a current density higher than 5.5 A m^{-2}, the potential drop of N/S-CNS is less steep than that of Pt/C, indicating a lower potential loss upon mass transfer.[50] This result, which implies a more efficient interaction between O_2 and N/S-CNS, together with the high specific surface area (1004 m^2 g^{-1}) and the comparable current generation in the MFC, suggests that mass transfer is playing a critical role in the overall cell performance in real applications.

While the power density of N/S-CNS is 34.8% lower than that of Pt/C, the comparable current density of N/S-CNS produced by the MFC (9.6% lower than that of Pt/C) indicates

DOI: 10.1021/acsami.5b05144
ACS Appl. Mater. Interfaces 2015, 7, 18672−18678

that the catalyst may be more suitable for current generation than for power production, and thus the application niches need to be identified. For example, a previous study suggested that a high current density was favorable for desalination in a microbial desalination cell (MDC),[51] which implies that N/S-CNS could be used as the cathode catalyst of MDCs for sustainable wastewater treatment and seawater desalination. Another advantage of N/S-CNS is the low cost. Given the yield of 41%, the cost of the catalyst for a 1 m^2 cathode is estimated to be approximately $168, which is remarkably lower than that of Pt/C ($2750). It is therefore expected that the capital cost of MFCs can be significantly reduced by the use of N/S-CNS.

CONCLUSIONS

In summary, we have demonstrated a simple synthesis procedure of codoped CNS with nitrogen and sulfur and investigated its performance for ORR in an MFC. The modified nanosheet catalyst shows pronounced electrocatalytic activity with enhanced ORR catalysis compared to the sole doping of nitrogen or sulfur. The excellent catalytic activities can be ascribed to the synergistic effect of the large surface area with abundant pores and N/S dual doping, the low ohmic and charge-transfer resistance, and the favorable four-electron pathway. The MFC equipped with N/S-CNS achieved current generation comparable to that with Pt/C, while the cost for N/S-CNS was more than 16 times lower than that of Pt/C. The results collectively represent a significant step toward the development of metal-free catalysts for MFCs.

AUTHOR INFORMATION

Corresponding Authors

*E-mail: jhchen@uwm.edu.
*E-mail: zhenhe@vt.edu.

Author Contributions

§These authors have contributed equally.

Notes

The authors declare no competing financial interest.

ACKNOWLEDGMENTS

Financial support for this work was provided by the U.S. Department of Energy (Grant DE-EE0003208), the Research Growth Initiative Program of the University of Wisconsin—Milwaukee, and a faculty startup fund from Virginia Tech. The authors thank Dr. Amanda Morris (Virginia Tech) for her help with RDE measurement.

REFERENCES

(1) Lee, K.; Zhang, L.; Zhang, J. *Pem Fuel Cell Electrocatalysts and Catalyst Layers*; Springer: London, 2008.
(2) Cao, Y. L.; Yang, H. X.; Ai, X. P.; Xiao, L. F. The Mechanism of Oxygen Reduction on Mno2-Catalyzed Air Cathode in Alkaline Solution. *J. Electroanal. Chem.* **2003**, *557*, 127−134.
(3) Zhao, F.; Harnisch, F.; Schröder, U.; Scholz, F.; Bogdanoff, P.; Herrmann, I. Application of Pyrolysed Iron(Ii) Phthalocyanine and Cotmpp Based Oxygen Reduction Catalysts as Cathode Materials in Microbial Fuel Cells. *Electrochem. Commun.* **2005**, *7*, 1405−1410.
(4) Edwards, R. S.; Coleman, K. S. Graphene Synthesis: Relationship to Applications. *Nanoscale* **2013**, *5*, 38−51.
(5) Lota, G.; Fic, K.; Frackowiak, E. Carbon Nanotubes and Their Composites in Electrochemical Applications. *Energy Environ. Sci.* **2011**, *4*, 1592−1605.
(6) Wang, H.; Maiyalagan, T.; Wang, X. Review on Recent Progress in Nitrogen-Doped Graphene: Synthesis, Characterization, and Its Potential Applications. *ACS Catal.* **2012**, *2*, 781−794.
(7) De Volder, M. F.; Tawfick, S. H.; Baughman, R. H.; Hart, A. J. Carbon Nanotubes: Present and Future Commercial Applications. *Science* **2013**, *339*, 535−539.
(8) Yang, B.; Yu, C.; Yu, Q.; Zhang, X.; Li, Z.; Lei, L. N-Doped Carbon Xerogels as Adsorbents for the Removal of Heavy Metal Ions from Aqueous Solution. *RSC Adv.* **2015**, *5*, 7182−7191.
(9) Ghasemi, M.; Daud, W. R. W.; Hassan, S. H. A.; Oh, S.-E.; Ismail, M.; Rahimnejad, M.; Jahim, J. M. Nano-Structured Carbon as Electrode Material in Microbial Fuel Cells: A Comprehensive Review. *J. Alloys Compd.* **2013**, *580*, 245−255.
(10) Xiao, L.; Damien, J.; Luo, J.; Jang, H. D.; Huang, J.; He, Z. Crumpled Graphene Particles for Microbial Fuel Cell Electrodes. *J. Power Sources* **2012**, *208*, 187−192.
(11) Paraknowitsch, J. P.; Thomas, A. Doping Carbons Beyond Nitrogen: An Overview of Advanced Heteroatom Doped Carbons with Boron, Sulphur and Phosphorus for Energy Applications. *Energy Environ. Sci.* **2013**, *6*, 2839−2855.
(12) Yang, Z.; Yao, Z.; Li, G.; Fang, G.; Nie, H.; Liu, Z.; Zhou, X.; Chen, X. a.; Huang, S. Sulfur-Doped Graphene as an Efficient Metal-Free Cathode Catalyst for Oxygen Reduction. *ACS Nano* **2012**, *6*, 205−211.
(13) Wohlgemuth, S.-A.; White, R. J.; Willinger, M.-G.; Titirici, M.-M.; Antonietti, M. A One-Pot Hydrothermal Synthesis of Sulfur and Nitrogen Doped Carbon Aerogels with Enhanced Electrocatalytic Activity in the Oxygen Reduction Reaction. *Green Chem.* **2012**, *14*, 1515−1523.
(14) Liang, J.; Jiao, Y.; Jaroniec, M.; Qiao, S. Z. Sulfur and Nitrogen Dual-Doped Mesoporous Graphene Electrocatalyst for Oxygen Reduction with Synergistically Enhanced Performance. *Angew. Chem., Int. Ed.* **2012**, *51*, 11496−11500.
(15) Liu, Z.; Nie, H.; Yang, Z.; Zhang, J.; Jin, Z.; Lu, Y.; Xiao, Z.; Huang, S. Sulfur-Nitrogen Co-Doped Three-Dimensional Carbon Foams with Hierarchical Pore Structures as Efficient Metal-Free Electrocatalysts for Oxygen Reduction Reactions. *Nanoscale* **2013**, *5*, 3283−3288.
(16) McCarty, P. L.; Bae, J.; Kim, J. Domestic Wastewater Treatment as a Net Energy Producer−Can This Be Achieved? *Environ. Sci. Technol.* **2011**, *45*, 7100−7106.
(17) Li, W.-W.; Yu, H.-q.; He, Z. Towards Sustainable Wastewater Treatment by Using Microbial Fuel Cells-Centered Technologies. *Energy Environ. Sci.* **2014**, *7*, 911−924.
(18) Logan, B. E. Exoelectrogenic Bacteria That Power Microbial Fuel Cells. *Nat. Rev. Microbiol.* **2009**, *7*, 375−381.
(19) Logan, B. E.; Hamelers, B.; Rozendal, R.; Schröder, U.; Keller, J.; Freguia, S.; Aelterman, P.; Verstraete, W.; Rabaey, K. Microbial Fuel Cells: Methodology and Technology. *Environ. Sci. Technol.* **2006**, *40*, 5181−5192.
(20) Dong, H.; Yu, H.; Wang, X. Catalysis Kinetics and Porous Analysis of Rolling Activated Carbon-Ptfe Air-Cathode in Microbial Fuel Cells. *Environ. Sci. Technol.* **2012**, *46*, 13009−13015.
(21) Zhang, B.; Wen, Z.; Ci, S.; Mao, S.; Chen, J.; He, Z. Synthesizing Nitrogen-Doped Activated Carbon and Probing Its Active Sites for Oxygen Reduction Reaction in Microbial Fuel Cells. *ACS Appl. Mater. Interfaces* **2014**, *6*, 7464−7470.
(22) Wang, X.; Feng, C.; Ding, N.; Zhang, Q.; Li, N.; Li, X.; Zhang, Y.; Zhou, Q. Accelerated Oh− Transport in Activated Carbon Air Cathode by Modification of Quaternary Ammonium for Microbial Fuel Cells. *Environ. Sci. Technol.* **2014**, *48*, 4191−4198.
(23) Yuan, H.; He, Z. Graphene-Modified Electrodes for Enhancing the Performance of Microbial Fuel Cells. *Nanoscale* **2015**, *7*, 7022−7029.
(24) Sevilla, M.; Fuertes, A. B. Direct Synthesis of Highly Porous Interconnected Carbon Nanosheets and Their Application as High-Performance Supercapacitors. *ACS Nano* **2014**, *8*, 5069−5078.

DOI: 10.1021/acsami.5b05144
ACS Appl. Mater. Interfaces 2015, 7, 18672−18678

(25) Yuan, H.; Li, J.; Yuan, C.; He, Z. Facile Synthesis of Mos2@Cnt as an Effective Catalyst for Hydrogen Production in Microbial Electrolysis Cells. *ChemElectroChem* **2014**, *1*, 1828−1833.
(26) Bard, A. J.; Faulkner, L. R. *Electrochemical Methods: Fundamentals and Applications*; Wiley: New York, 1980; Vol. 2.
(27) Phillips, S. L. Potentiostatic Determination of Diffusion Coefficient of Oxygen in Absence and Presence of Surfactants. *Anal. Chem.* **1966**, *38*, 1714−1719.
(28) He, Z.; Wagner, N.; Minteer, S. D.; Angenent, L. T. An Upflow Microbial Fuel Cell with an Interior Cathode: Assessment of the Internal Resistance by Impedance Spectroscopy. *Environ. Sci. Technol.* **2006**, *40*, 5212−5217.
(29) Hou, Y.; Zhang, B.; Wen, Z.; Cui, S.; Guo, X.; He, Z.; Chen, J. A 3d Hybrid of Layered Mos2/Nitrogen-Doped Graphene Nanosheet Aerogels: An Effective Catalyst for Hydrogen Evolution in Microbial Electrolysis Cells. *J. Mater. Chem. A* **2014**, *2*, 13795−13800.
(30) Yang, S.; Zhi, L.; Tang, K.; Feng, X.; Maier, J.; Müllen, K. Efficient Synthesis of Heteroatom (N or S)-Doped Graphene Based on Ultrathin Graphene Oxide-Porous Silica Sheets for Oxygen Reduction Reactions. *Adv. Funct. Mater.* **2012**, *22*, 3634−3640.
(31) Hou, Y.; Li, J.; Wen, Z.; Cui, S.; Yuan, C.; Chen, J. Co3o4 Nanoparticles Embedded in Nitrogen-Doped Porous Carbon Dodecahedrons with Enhanced Electrochemical Properties for Lithium Storage and Water Splitting. *Nano Energy* **2015**, *12*, 1−8.
(32) Hou, Y.; Zuo, F.; Dagg, A.; Feng, P. Visible Light-Driven A-Fe2o3 Nanorod/Graphene/Biv1−Xmoxo4 Core/Shell Heterojunction Array for Efficient Photoelectrochemical Water Splitting. *Nano Lett.* **2012**, *12*, 6464−6473.
(33) Yang, W.; Liu, X.; Yue, X.; Jia, J.; Guo, S. Bamboo-Like Carbon Nanotube/Fe3c Nanoparticle Hybrids and Their Highly Efficient Catalysis for Oxygen Reduction. *J. Am. Chem. Soc.* **2015**, *137*, 1436−1439.
(34) Wen, Z.; Ci, S.; Hou, Y.; Chen, J. Facile One-Pot, One-Step Synthesis of a Carbon Nanoarchitecture for an Advanced Multifunctonal Electrocatalyst. *Angew. Chem., Int. Ed.* **2014**, *53*, 6496−6500.
(35) Jin, Z.-Y.; Lu, A.-H.; Xu, Y.-Y.; Zhang, J.-T.; Li, W.-C. Ionic Liquid-Assisted Synthesis of Microporous Carbon Nanosheets for Use in High Rate and Long Cycle Life Supercapacitors. *Adv. Mater.* **2014**, *26*, 3700−3705.
(36) Hou, Y.; Wen, Z.; Cui, S.; Ci, S.; Mao, S.; Chen, J. An Advanced Nitrogen-Doped Graphene/Cobalt-Embedded Porous Carbon Polyhedron Hybrid for Efficient Catalysis of Oxygen Reduction and Water Splitting. *Adv. Funct. Mater.* **2015**, *25*, 872−882.
(37) Niu, W.; Li, L.; Liu, X.; Wang, N.; Liu, J.; Zhou, W.; Tang, Z.; Chen, S. Mesoporous N-Doped Carbons Prepared with Thermally Removable Nanoparticle Templates: An Efficient Electrocatalyst for Oxygen Reduction Reaction. *J. Am. Chem. Soc.* **2015**, *137*, 5555−5562.
(38) Gao, S.; Liu, H.; Geng, K.; Wei, X. Honeysuckles-Derived Porous Nitrogen, Sulfur, Dual-Doped Carbon as High-Performance Metal-Free Oxygen Electroreduction Catalyst. *Nano Energy* **2015**, *12*, 785−793.
(39) Ito, Y.; Cong, W.; Fujita, T.; Tang, Z.; Chen, M. High Catalytic Activity of Nitrogen and Sulfur Co-Doped Nanoporous Graphene in the Hydrogen Evolution Reaction. *Angew. Chem., Int. Ed.* **2015**, *54*, 2131−2136.
(40) Ma, X.; Ning, G.; Sun, Y.; Pu, Y.; Gao, J. High Capacity Li Storage in Sulfur and Nitrogen Dual-Doped Graphene Networks. *Carbon* **2014**, *79*, 310−320.
(41) Wen, Z.; Wang, X.; Mao, S.; Bo, Z.; Kim, H.; Cui, S.; Lu, G.; Feng, X.; Chen, J. Crumpled Nitrogen-Doped Graphene Nanosheets with Ultrahigh Pore Volume for High-Performance Supercapacitor. *Adv. Mater.* **2012**, *24*, 5610−5616.
(42) Xu, J.; Wang, M.; Wickramaratne, N. P.; Jaroniec, M.; Dou, S.; Dai, L. High-Performance Sodium Ion Batteries Based on a 3d Anode from Nitrogen-Doped Graphene Foams. *Adv. Mater.* **2015**, *27*, 2042−2048.
(43) Lee, K. R.; Lee, K. U.; Lee, J. W.; Ahn, B. T.; Woo, S. I. Electrochemical Oxygen Reduction on Nitrogen Doped Graphene Sheets in Acid Media. *Electrochem. Commun.* **2010**, *12*, 1052−1055.
(44) Su, Y.; Zhang, Y.; Zhuang, X.; Li, S.; Wu, D.; Zhang, F.; Feng, X. Low-Temperature Synthesis of Nitrogen/Sulfur Co-Doped Three-Dimensional Graphene Frameworks as Efficient Metal-Free Electrocatalyst for Oxygen Reduction Reaction. *Carbon* **2013**, *62*, 296−301.
(45) Xiao, M.; Zhu, J.; Feng, L.; Liu, C.; Xing, W. Meso/Macroporous Nitrogen-Doped Carbon Architectures with Iron Carbide Encapsulated in Graphitic Layers as an Efficient and Robust Catalyst for the Oxygen Reduction Reaction in Both Acidic and Alkaline Solutions. *Adv. Mater.* **2015**, *27*, 2521−2527.
(46) Hou, Y.; Huang, T.; Wen, Z.; Mao, S.; Cui, S.; Chen, J. Metal−Organic Framework-Derived Nitrogen-Doped Core-Shell-Structured Porous Fe/Fe3c@C Nanoboxes Supported on Graphene Sheets for Efficient Oxygen Reduction Reactions. *Adv. Energy Mater.* **2014**, *4*,10.1002/aenm.201400337.
(47) Wang, X.; Wang, J.; Wang, D.; Dou, S.; Ma, Z.; Wu, J.; Tao, L.; Shen, A.; Ouyang, C.; Liu, Q.; Wang, S. One-Pot Synthesis of Nitrogen and Sulfur Co-Doped Graphene as Efficient Metal-Free Electrocatalysts for the Oxygen Reduction Reaction. *Chem. Commun.* **2014**, *50*, 4839−4842.
(48) You, C.; Liao, S.; Li, H.; Hou, S.; Peng, H.; Zeng, X.; Liu, F.; Zheng, R.; Fu, Z.; Li, Y. Uniform Nitrogen and Sulfur Co-Doped Carbon Nanospheres as Catalysts for the Oxygen Reduction Reaction. *Carbon* **2014**, *69*, 294−301.
(49) Gong, K.; Du, F.; Xia, Z.; Durstock, M.; Dai, L. Nitrogen-Doped Carbon Nanotube Arrays with High Electrocatalytic Activity for Oxygen Reduction. *Science* **2009**, *323*, 760−764.
(50) Zhao, F.; Slade, R. C.; Varcoe, J. R. Techniques for the Study and Development of Microbial Fuel Cells: An Electrochemical Perspective. *Chem. Soc. Rev.* **2009**, *38*, 1926−39.
(51) Jacobson, K. S.; Drew, D. M.; He, Z. Use of a Liter-Scale Microbial Desalination Cell as a Platform to Study Bioelectrochemical Desalination with Salt Solution or Artificial Seawater. *Environ. Sci. Technol.* **2011**, *45*, 4652−7.

DOI: 10.1021/acsami.5b05144
ACS Appl. Mater. Interfaces 2015, 7, 18672−18678